Molecular mechanism of analgesic bias on μ-opioid receptor

Yi Sun[1], Wenli Wang[2], Shuai Shao[1], Xiangyun Tian[1], Yulei Li[1], Bo Tan[1], Wei Fu[2], and Ruibin Su[1]

[1]Beijing Institute of Pharmacology and Toxicology
[2]Fudan University School of Pharmacy

May 5, 2020

Abstract

Background and Purpose The development of biased agonism provides a promising avenue to improve the pharmacological properties of fentanyl derivatives, but the molecular mechanism underlying ligand bias still remains ambiguous. Therefore, we sought to find out the critical sites of μ-receptor governing ligand bias and clarify corresponding molecular mechanism for designing and synthesizing effective analgesics with reduced adverse effects. Experimental Approach Critical sites governing ligand bias were identified both by computational prediction and cell assay-based bias analysis on wild-type and site-directed mutant μ-opioid receptor. Then molecular dynamics simulations of wild-type and mutant μ-opioid receptor were conducted to investigate the mechanism of bias activation. Key Results D3.32A and H6.52L mutation disrupted the binding of fentanyl derivatives with μ-opioid receptor. W6.48L mutation drove most fentanyl derivatives to β-arrestin-bias but promote sufentanil to cAMP signaling-bias. The result of molecular dynamics simulation showed that W6.48 and Y7.43 were paired activation switches of ligand bias at μ-opioid receptor. Conclusion and Implications D3.32 and H6.52 were critical residues in driving morphine and fentanyl derivatives to bind with μ-opioid receptor. W6.48 was a pivotal residue in governing the bias signaling and the interactions of ligands with W6.48 and Y7.43 were the structural determinants for the signaling bias of μ-opioid receptor, which will be conducive for better design and synthesis of effective opioid analgesics with the reduced adverse effects.

Abstract

Background and Purpose

The development of biased agonism provides a promising avenue to improve the pharmacological properties of fentanyl derivatives, but the molecular mechanism underlying ligand bias still remains ambiguous. Therefore we sought to find out the critical sites of μ-receptor governing ligand bias and clarify corresponding molecular mechanism for designing and synthesizing effective analgesics with reduced adverse effects.

Experimental Approach

Critical sites governing ligand bias were identified both by computational prediction and cell assay-based bias analysis on wild-type and site-directed mutant μ-opioid receptor. Then molecular dynamics simulations of wild-type and mutant μ-opioid receptor were conducted to investigate the mechanism of bias activation.

Key Results

D3.32A and H6.52L mutation disrupted the binding of fentanyl derivatives with μ-opioid receptor. W6.48L mutation drove most fentanyl derivatives to β-arrestin-bias but promote sufentanil to cAMP signaling-bias. The result of molecular dynamics simulation showed that W6.48 and Y7.43 were paired activation switches of ligand bias at μ-opioid receptor.

Conclusion and Implications

D3.32 and H6.52 were critical residues in driving morphine and fentanyl derivatives to bind with μ-opioid receptor. W6.48 was a pivotal residue in governing the bias signaling and the interactions of ligands with W6.48 and Y7.43 were the structural determinants for the signaling bias of μ-opioid receptor, which will be conducive for better design and synthesis of effective opioid analgesics with the reduced adverse effects.

Fentanyl derivatives | ligand bias | μ-opioid receptor | molecular dynamics simulations | biased mechanism

Morphine and fentanyl derivatives have been the world's most widely and frequently used opioid analgesics for decades(*1*). However, various adverse effects threaten the medication safety of morphine and fentanyl derivatives, such as gastrointestinal disorder, tolerance, dependence and respiratory depression etc(*2*). Notably, morphine and fentanyl derivatives have been evolved in the global public health threat recent years for an unprecedented rise of death due to respiratory depression caused by overdose(*3* ,*4*). Consequently, unremitting efforts have been directed towards seeking novel opioid analgesics with improved therapeutic profiles.

A recent development in theory of biased agonism at μ-opioid receptor (MOR) provides a promising avenue for therapeutic improvement. It is reported that both desirable and adverse effects of morphine and fentanyl derivatives are attributed to the activation of MOR(*5*). As other G-protein-coupled receptors (GPCRs), two parallel signaling pathways mediated the function of MOR through its activation, one is G protein-dependent signaling and the other is β-arrestin-dependent signaling. A series of β-arrestin-knockout mice experiments displayed enhanced and prolonged morphine-induced antinociception with attenuated respiratory suppression(*6-10*). Recent research indicated that β-arrestin-biased compounds of morphine and fentanyl derivatives are devoted to the respiratory depression while G protein-bias pathway is responsible for the antinociception(*11*). These findings showed that MOR agonists preferentially biased towards G protein signaling over β-arrestin signaling exert analgesia with reduced unwanted fatal side effects. The discovery of several G-protein biased compounds proves the rationality and practicality of biased agonism theory, such as PZM21 and TRV130(*12*) (*13*), which were promising potential novel analgesics.

The molecular mechanism underlying biased agonism still remains ambiguous. Recent crystal structure analyses of MOR displayed the binding modes of MOR with agonists(*14* ,*15*), which suggested that different ligands may induce diverse multiple stable receptor conformations that leads to variety degrees of activation of downstream signaling pathways. Jeffrey S. Smith advanced a ternary complex model to explain the factors resulted in the development of biased response, allosterically interpret the interactions of receptors with ligand and transducer(*16*). The intermediate conformational state of receptor induced by ligand decides either transducer-G protein or β-arrestin is needed for stabilization of the ternary complex. Researches of other GPCR, such as neuropeptide Y1 and Y4 receptor, CXC-chemokine receptor 4 and 7, suggested that distinct amino acid within the receptor can influence the downstream signaling bias(*17* ,*18*). Hence, there may be some crucial residues in MOR within core binding region accounting for biased agonism, and these residues are the breakthrough to explore the mechanism underlying the development of signaling bias, which will direct the design and syntheses of desirable biased ligands. In this study, the mutation experiments and cell-based G-protein and β-arrestin assays are in combination with computational modeling studies were used to identify the key residues governing ligand bias and to clarify the molecular mechanism underlying biased agonism.

Method

Homology modeling

The homo sapiens active μ opioid receptor was built by taking the X-ray structure of musculus active μ opioid receptor (PDB code: 5C1M) as a template by using the homology modeling module of Discovery Studio 3.5 software(*15*). All water molecules in the X-ray structure were retained. Ramachandran plot was employed

to evaluate the validity of the homology models in **Figure S1** . Residues were numbered according to the generalized numbering scheme proposed by Ballesteros and Weinstein(*19*).

Molecular docking

The morphine, fentanyl and sufentanil were docked into the 3D structure of homo sapiens active μ opioid receptor. We used the Glide Docking module in Maestro 3.5 program to dock these compounds into the binding site of the active μ opioid receptor. These three systems were subjected to Monte Carlo Multiple Minimum conformational searches using the OPLS_2005 force field. The minimized conformations were selected for the next molecular dynamics simulations.

Molecular dynamic simulations

Eight systems were built for molecular dynamics simulations: (1) μ opioid receptor without ligand (Apo); (2) morphine-bound active MOR; (3) sufentanil-bound active MOR; and (4) fentanyl-bound active MOR; (5) mutant μ opioid receptor without ligand (Apo-W6.48L); (6) morphine-bound active mutant MOR (W6.48L); (7) sentinel-bound active mutant MOR (W6.48L); and (8) fentanyl-bound mutant MOR (W6.48L). MD simulations were performed using the Gromacs5.1.2 package. All systems were embedded in a hydrated POPC lipid bilayer. Water molecules were used to solvate the protein. After that, Na^+ and Cl^- ions were added in the water to neutralize the system using 0.15 mol/L NaCl. The steepest descent followed by conjugate gradient methods were used for the energy minimization for these systems. Then, we gradually heated the systems from 0 K to 310 K. The systems were subjected to equilibrate at constant pressure and temperature for 1 ns (310 K, 1 atm). Finally, the production MD simulations of eight systems were performed for 100 ns. All analyses of MD trajectories were performed using the tools implemented in the Gromacs5.1.2 package.

Plasmid construction and site-directed mutagenesis

To make wild-type and mutant (WT & mutant) MOR plasmids, full-length hOPRM1 cDNA was subcloned into the Tag-lite® pT8-SNAP vector (Cisbio, France). The Vazyme® Fast Mutagenesis Kit V2 (Vazyme, China)was used to introduce the D3.32A, W6.48L, H6.52L site mutation to the MOR recombinant plasmid, the nucleotide sequences of mutant MOR were confirmed by DNA sequencing and sequence alignment. Primers designed to amplify MOR plasmid containing mutant site are listed here:

D3.32A

F 5'-TCCATAG*C* TTACTATAACATGTTCACCAGC-3'

R 5'-ATAGTAA*G* CTATGGAGATCACTATCTTGCA-3'

W6.48L

F 5'-GTCTGCT*T* GACTCCCATTCACATTTACGTC-3'

R 5'-GGGAGTC*A* AGCAGACGATGAACACAGCCAC-3'

H6.52L

F 5'-CCCATTC*T* CATTTACGTCATCATTAAAGCC-3'

R 5'-GTAAATG*A* GAATGGGAGTCCAGCAGACGAT-3'

Cell lines

Chinese Hamster Ovary (CHO-K1) cells were purchased from ATCC and maintained in F12 medium containing 10% fetal bovine serum (FBS).

To obtain CHO stably expressing MOR (WT & mutant) cell lines, wild-type and D3.32A, W6.48L, H6.52L mutant MOR plasmids were respectively transfected into CHO-K1 cells using lipofectamine$^{(r)}$ LTX regent. The transfected cell mixtures were grown under the selection pressure of 200 μg/ml hygromycin for 10 days, then cells were seeded in 96-well plates at an approximate density of 1 cell per well to isolate clones. An appropriate clone was selected for further experimental studies. The MOR expression of CHO-MOR cell lines was confirmed by western-blot analysis (**Figure S3A**). To verify the site mutation of each CHO-MOR cell line, we amplified the target MOR fragments from total genomic DNA (**Figure S3B**). Then DNA sequencing analysis of the PCR products verified the correct site mutation of MOR in CHO-MOR cell lines. Membrane MOR expression of the CHO-MOR cell lines was measured by immunofluorescence analysis (**Figure S3D**). The expression level of wild-type and D3.32A MOR on membranes was confirmed to be similar, and the W6.48L and H6.52L mutant MOR is approximately 63% of wild-type. CHO-MOR (WT & mutant) cells were maintained in F12 medium supplemented with 10% FBS and 40 μg/ml hygromycin.

To obtain CHO-stably expressing both MOR (WT & mutant) and β-arrestin2-EGFP cell lines, we transfected the β-arrestin2-EGFP plasmid into each CHO-MOR (WT & mutant) cell line. After growing under the selection pressure of 6 μg/ml puromycin for 10 days, cell mixtures were seeded in 96-well plates at an approximate density of 1 cell per well to isolate clones. An appropriate clone was selected for further experiments. The expression of β-arrestin2 was verified by western-blot analysis and the expression level of each cell line was confirmed to be similar (**Figure S3C**). CHO-MOR (WT & mutant)-β-arrestin2-EGFP cells were maintained in F12 medium supplemented with 10% FBS and 40 μg/ml hygromycin and 2 μg/ml puromycin.

All cells were cultured according to the standard protocol in 37 incubator with 5% CO2.

Western-blot

Adherent CHO cells expressing MOR (WT & mutant) or β-arrestin2 were lysed in RIPA lysis buffer (50 mM pH 7.4 Tris, 150 mM NaCl, 1% Triton X-100, 1% sodium deoxycholate, 0.1% SDS) supplemented with protease inhibitor cocktail and phosphatase inhibitor. The lysate was incubated at 37 for 10 min, then separated by SDS-PAGE of 8% polyacrylamide gels and transferred to PVDF membranes. Membranes were immunoblotted with anti-MOR antibody (Millipore, AB1580-I) to verify the expression of MOR or immunoblotted with anti-β-arrestin 2 antibody (Cell signaling technology, 3857) to verify the expression of β-arrestin 2. To ensure equal loading into each lane, blots were also incubated with GAPDH antibody.

Immunofluorescence

Membrane MOR can be labelled with SNAP-Lumi4-Tb, and MOR-Tb level could be quantified by Envision Multilabel Reader at 615 nm. CHO-MOR (WT & mutant) cells were seeded on 35 mm dishes and grown to 80% confluence. Cells were incubated with SNAP-Lumi4-Tb solution (Cisbio, France) for 1 h. Then cells were digested and dispensed into 384-well plate at a density of 20000 cells per well, and the total test volume is 20 μl. Read the plate on Envision Multilabel Reader (Perkin Elmer) at 615 nm. The response represents the expression level of MOR.

Genomic DNA PCR

CHO-MOR (WT & mutant) cells were seeded on 35 mm dishes and grown to 80% confluence. Genomic DNA was extracted from cells using the Gentra pure gene cell kit (Qiagen, Germany). MOR DNA fragments were amplified from genomic DNA by PCR primers F: 5'-CTCGCCGTGAAAGAGTGGCT-3', R: 5'-GGGCAACGGAGCAGTTTCT-3'. Then the PCR products were sequenced to verify the mutant site.

Radioligand saturation binding assay

Radioligand saturation binding assay was performed to determine the affinity of fentanyl in binding with MOR. Membrane proteins were extracted from CHO cells expressing MOR (WT & mutant), and 20 μg proteins were used for each reaction. In specific binding reaction, membranes were incubated with a series of concentrations of [^{3}H]Fentanyl (ranging from 1.5625 nM to 50 nM) for 30 min at 37 in Tris-HCl buffer (50 mM Tris, pH 7.4). In nonspecific binding reaction, membranes were incubated with 5 μM naloxone and [^{3}H]Fentanyl (ranging from 1.5625 nM to 50 nM) for 30 min at 37 in Tris-HCl buffer. The reaction mixtures were filtered over GF/C filters, and then the filters were washed three times by cold Tris-HCl buffer. Radioactivity was assayed by liquid scintillation counting overnight.

HTRF competitive binding assay

HTRF competitive binding assay was performed according to the Tag-lite® binding assay recommended protocol (Cisbio, France). This assay is based on the competition between the Tag-lite® fluorescent ligand and test compounds. CHO-MOR (WT & mutant) cells were labeled in batch with SNAP-Lumi4-Tb and suspended in Tag-lite® labeling buffer (TLB), then cells dispensed into 384 well small volume white plate (Thermo Scientific Nunc, USA) at a density of 5000 cells per well. To determine saturation binding constant Kd of the fluorescent ligand, cells were incubated with a series of concentrations (ranging from 0.1 nM to 100 nM) of the fluorescent ligand in TLB. Non-specific binding signal wells were incubated with 100 nM Naltrindole. For competition binding experiments, cells were incubated with varying concentrations (ranging from 10-4 M to 10-14 M) of test compounds in the presence of 8 nM fluorescent ligand. The total binding reaction volume is 20 μl, and the concentration mentioned above means final concentration. Read the plate on Envision Multilabel Reader (Perkin Elmer) at 665 nm and 615 nm after 3 h incubation. The HTFR ratio was calculated as the equation:

$$HTRF\ Ratio = \frac{Signal\ 665\ nm}{Signal\ 615\ nm} \times 10^4 \#Equation\ 1$$

cAMP assay

The cAMP assay was performed according to the cAMP-Gi kit protocol (Cisbio, France). CHO-MOR (WT & mutant) cells were harvested and suspended in stimulation buffer supplemented with 0.5 mM IBMX. Then cells were dispensed into 384-well small volume white plate (Thermo Scientific Nunc, USA) at a density of 5000 cells per well. Add a series of concentrations (ranging from 10^{-12} M to 10^{-6} M) of test compounds and 3 μM forskolin into wells (non-stimulated control wells add stimulation buffer instead of test compounds at this step), seal the plate and incubate at room temperature (RT) for 15 min. Add cAMP-Cryptate and anti-cAMP-d2 working solution into wells, seal the plate and incubate at RT for 1 h. The total binding reaction volume is 20 μl, and the concentration mentioned above means final concentration. Read the plate on Envision Multilabel Reader (Perkin Elmer) at 665 nm and 615 nm after 3 h incubation. The response was calculated as **Equation 1** .

β-αρρεστιν2 ρεχρυιτμεντ ασσαψ

CHO-MOR (WT & mutant)-βarrestin2 cells were seeded into 96-well, black-walled, clear-bottom assay plate (Costar, USA) at an appropriate density to ensure they will be 50%˜70% confluent next day. For the assay, cells were serum-starved for 1 h, then treated with a series of concentrations (ranging from 10^{-12} M to 10^{-5} M) of test compounds for 5 min at 37 . Cells were fixed and dyed using 4% paraformaldehyde (PFA) with Hoechst nuclear stain (1:10000) for 30 min. β-arrestin2 translocation images were captured with a 20× objective on an ArrayScan XTI High Content Analysis (HCA) Reader (Thermo Scientific, USA). The spots/nuclear ratio per well was quantified using Cellomics Spot(r) Detection BioApplication (Thermo Scientific, USA).

Data analysis and statistical procedures

GraphPad Prism (V7.0) software was used for curve fitting and data analysis. All data are shown as mean +- SEM of at least three independent experiments run in duplicate or triplicate.

For binding assays, concentration-response curves were fit to one-site binding models provided in Prism software to determine K_d, B_{max}, and K_i.

For functional assays, data are shown by subtracting basal values and presented as percentage of DAMGO, then were fit to a non-linear regression (three-parameter) model to determine EC_{50} and E_{max}. As indicated, the difference between all the fitting parameters of wild-type MOR versus W6.48L mutant MOR was acquired via unpaired, two-tailed t-test.

We used the classic operational model analysis method to calculate ligand bias. The operational model (Black and Leff, 1983)(*20*) was applied to calculate bias as described by van der Westhuizen et al. (2014) (*21*)and Laura M. Bohn et al. (2017)(*22*). The transduction ratio (τ/KA) was determined based on the equation:

$$E = \frac{E_{\max}}{1+\left(\frac{1+\frac{A}{10^{\log\left(K_A\right)}}}{A\times 10^{\log\left(\frac{\tau}{K_A}\right)}}\right)^n} \#Equation\ 2$$

Where E is the effect of ligand, E_{max} is the maximal response, A is the molar concentration of the ligand, $K_A$is the equilibrium dissociation constant, and the $\log(\tau/K_A)$ is the transduction coefficient(*21* ,*23*). For each assay, the E_{max} is constrained to be a shared value, the basal is constrained to be the value of zero and n is constrained to the value of 1.

DAMGO was chosen as the reference ligand. To eliminate system deviation, the Δ log (τ/K_A) of test ligand and SEM were calculated by **Equation 3** and **Equation 4** :

$$\log\left(\frac{\tau}{K_A}\right) = \log\left(\frac{\tau}{K_A}\right)_{\text{test}} - \log\left(\frac{\tau}{K_A}\right)_{\text{DAMGO}} \#\text{Equation 3}$$

$$\Sigma E_{\left(\Delta\ \lambda o\gamma\left(\frac{\tau}{K_A}\right)\right)} = \sqrt{\left(SE_{\left(\log\left(\frac{\tau}{K_A}\right)\right)_{\text{test}}}\right)^2 + \left(SE_{\left(\log\left(\frac{\tau}{K_A}\right)\right)_{\text{DAMGO}}}\right)^2} \#Equation\ 4$$

The bias parameter $\Delta\Delta$ log (τ/K_A) and SEM were calculated by **Equation 5** and **Equation 6** :

$$\log\left(\frac{\tau}{K_A}\right)_{\frac{\text{cAMP}}{\beta arr2}} = \log\left(\frac{\tau}{K_A}\right)_{\text{cAMP}} - \log\left(\frac{\tau}{K_A}\right)_{\beta arr2} \#\text{Equation 5}$$

$$\Sigma E_{\left(\Delta\Delta\ \lambda o\gamma\left(\frac{\tau}{K_A}\right)\right)} = \sqrt{\left(\Sigma E_{\left(\Delta\ \lambda o\gamma\left(\frac{\tau}{K_A}\right)\right)_{test:cAMP}}\right)^2 + \left(\Sigma E_{\left(\Delta\ \lambda o\gamma\left(\frac{\tau}{K_A}\right)\right)_{test:\beta arr2}}\right)^2} \#\text{Equation 6}$$

Materials

[^{3}H]Fentanyl was purchased from Perkin Elmer (USA). DAMGO and Naltrindole were purchased from Tocris (UK). Forskolin and 3-isobutyl-1-methylxanthine (IBMX) were purchased from Sigma-Aldrich (USA). Morphine was purchased from QINHAI pharmaceutical factory (China). Fentanyl derivatives were synthesized by our institute. Cell culture reagents were purchased from Gibco (USA).

Result

Τηε βινδινγ μοδες οφ μ-οπιοιδ ρεχεπτορ ωιτη μορπηινε, φεντανψλ ανδ συφεντανιλ

The 3D model of homo sapiens active μ opioid receptor was constructed based on the crystal structure of mouse active μ opioid receptor (PDB code: 5c1m)(*15*) and shown in**Figure S1A** , 91.2% amino acids (270aa/296aa) located in the additional allowed regions in Ramachandran plot (**Figure S1B**). The molecular docking followed by molecular dynamics simulations identified the accurate binding modes of μ opioid receptor with morphine, fentanyl and sufentanil. These three binding modes were representative structures which accounted for the largest group in cluster analysis.

As shown in **Figure 1A˜C,** the protonated nitrogen atom of three drug molecules forms a strong salt bridge with the carboxyl oxygen atom of residue D3.32 in μ opioid receptor, though the structure of morphine is completely different from that of fentanyl and sufentanil. In addition, the role of H6.52 was identified: the epoxy group of morphine interacted with the imidazole side chain of H6.52 through the water bridge. At the same time, the phenolic hydroxyl group of morphine formed a hydrogen bond with the nitrogen atom of the imidazole ring in H6.52. In terms of the binding mode of fentanyl and sufentanil with MOR, the oxygen of amide forms the hydrogen bond network with the side chains of H6.52 through water bridges. Therefore, these two residues were selected to mutate to investigate their role in the binding and biased agonism. Another important residue W6.48 was identified to be a molecular switch in the activation of MOR. W6.48 was relatively far from the active pocket and does not have direct interaction with the ligand, while its role was identified by MD simulations in adjusting the signal transduction of G-protein or β-arrestin. Therefore, D3.32, H6.52, and W6.48 were selected to mutate and test their biased signals in order to investigate their roles in the biased mechanism.

Ω6.48 ις α χριτιχαλ σιτε ινφλυενχινγ λιγανδ βιας ατ μ-οπιοιδ ρεχεπτορ

We developed CHO stably expressing MOR (wild-type and D3.32A, W6.48L, H6.52L mutant) cell lines to explore the role of these three sites in the interaction between ligand and μ-opioid receptor.

The D3.32A and H6.52L mutation disrupted the binding of fentanyl with MOR in radioligand binding assay (**Figure 1D**), as well as the binding of the fluorescent ligand with MOR in HTRF binding assay (**Figure 1E**). Both in the cAMP assay and β-arrestin recruitment assay, the effects of test agonists to stimulate D3.32A and H6.52L mutant MOR were completely or notably decreased in comparison with wild-type MOR (**Figure S5C, D, G, H**). It did not contradict the results of binding assays and was in agreement with the binding mode that these two residues form hydrogen bond network with morphine, fentanyl, and sufentanil molecules. The D3.32A, and H6.52L mutations result in the breakdown of the hydrogen bond network, which interfered the ligand-receptor binding, thus led to completely loss in activity of MOR.

W6.48L mutation increased the affinity of fentanyl derivatives in binding with MOR. As shown in radioligand saturation binding curves (**Figure 1D**), the affinity of [3H]fentanyl in binding with the W6.48L mutant MOR (K_d = 0.23 ± 0.03 nM) was stronger than that of the wild-type MOR (K_d = 1.07 ± 0.21 nM). Then we performed HTRF binding assay to test the affinity of a series of fentanyl derivatives in binding with MOR and determined the differences between the affinity of W6.48L mutant MOR and wild-type MOR. In HTRF saturation binding, there was no significant difference observed between the K_d value of W6.48L mutant MOR and wild-type MOR via unpaired, two-tailed t-test, which enabled the following determined K_i and B_{max} values of wild-type and W6.48L mutant MOR to be statistically comparable. The competition binding curves showed that W6.48L mutation did not block the binding of test agonists with MOR (**Figure 1G**). The corresponding K_i values of test agonists for wild-type and W6.48L mutant MOR were shown in **Table 1** . Unlike classic MOR ligands DAMGO and morphine, fentanyl derivatives showed stronger affinity at W6.48L mutant MOR over the wild-type. Collectively, W6.48L mutation promoted the binding of fentanyl derivatives with MOR.

We carried out the commercially available cAMP assay (**Figure 2A, C**) and β-arrestin recruitment assay (**Figure 2B, D**) to further investigate if W6.48L mutation influenced the functional activity of fentanyl derivatives to stimulate MOR-mediated G-protein-dependent signaling and β-arrestin-dependent signaling. As shown in **Table 1** , the potencies of morphine, DAMGO and fentanyl to activate cAMP assay for W6.48L mutant MOR were lower than wild-type MOR. The efficacies of fentanyl, sufentanil and remifentanil for W6.48L mutant MOR were significantly reduced versus the wild-type. It is suggested that W6.48L mutation decreased the activities of fentanyl derivatives to stimulate G-protein-dependent signaling. However, remifentanil and 3-methyfentany showed improved potency and efficacy to promote β-arrestin recruitment for W6.48L mutant MOR over the wild-type (**Table 1**), which indicated that W6.48L mutation increase the effects of fentanyl derivatives to activate β-arrestin-dependent signaling. Altogether, W6.48L mutation exerted contrary influences to G-protein-dependent signaling and β-arrestin-dependent signaling, suggesting that W6.48L changes the ligand bias of fentanyl derivatives at MOR.

To quantify the ligand bias of fentanyl derivatives, the operational model was applied to calculate the bias factor $\Delta\Delta\log(\tau/K_A)$(*21* ,*22*). We found that W6.48L mutation drove most test agonists relatively bias toward β-arrestin-dependent signaling except sufentanil (**Table 2**). It is important to note that W6.48L mutation had comparatively considerate but not identical impacts on morphine, fentanyl and sufentanil (**Figure 2E**). The mutation reduced the degree of G-protein-bias for morphine, made the G-protein-bias convert to β-arrestin-bias for fentanyl, while it made the β-arrestin-bias convert to G-protein-bias for sufentanil.

W6.48 acts as a structural determinant in adjusting the 3-7 lock

Above studys show that W6.48 is a critical site affecting ligand bias at MOR, but how the W6.48L mutation changes the ligand bias and why the mutation have varying impact on the three different ligands remain unknown. The molecular docking and molecular dynamics (MD) simulations were used to investigate the biased mechanism of morphine and fentanyl derivatives to activate MOR-mediated signaling.

The MD simulations showed that, for all of these systems, the temperature, mass density and volume are relatively stable after 2 ns, the fluctuations scale became much smaller for both the RMS deviations of the Cα atoms and potential energy of all of the systems (**Figure S2**), indicating that all of the molecular systems were well behaved.

It is reported that the states of 3-7 lock, which was formed by the hydrogen bond between D3.32 and Y7.43, that impacts the activation of MOR. The distance of 3-7 lock was monitored to examine if the close or open state of 3-7 lock is relative to the activation of wild and mutation MOR (**Figure 3**). In terms of wild type MOR-drug systems, the distance in 3-7 lock of sufentanil fluctuated from 0.4 to 0.6 nm after simulation of 10 ns, which is slightly longer than that of morphine and fentanyl's bound MORs. While in terms of drug-bound W6.48L mutant MORs, all distances among three systems tend to be smaller than 0.3 nm, i.e., the 3-7 lock is tightly closed, i.e. the strong interaction in TM3-TM7 was formed. Combining the biased signaling assay (**Figure 2**) and the time-evolved distance changes in 3-7 lock (**Figure 3**), the tight pairs were formed in morphine and fentanyl bound mutation systems. Correspondingly, the biased signalling is propitious to β-arresin; while the distance in 3-7 lock is larger than that of morphine and fentanyl's mutation systmes, the G-protein biased signaling is enhanced. In this process, 3-7 lock was adjusted by W6.48, that stabilized Y7.43 by forming paired stable hydrophobic interaction (**Figure 4**). It was indicated that W6.48 acted as a structural determinant in adjusting the 3-7 lock that functions as a molecular switch to activate the downstream signaling.

Ω6.48 ανδ Ψ7.43 ωερε παιρεδ αστιατιον σωιτσηες οφ λιγανδ βιας ατ μ-οπιοιδ ρεσεπτορ

By analyzing the processes of morphine, fentanyl and sufentanil interacting with MOR during the MD simulations as well as the above results of functional assays, we found that W6.48 and Y7.43 are the paired

activation switches in the biased signal transduction. The interactions of these two residues in MOR with morphine, fentanyl and sufentanil were shown in **Figure 1A-C** . The distances between W6.48 and the three ligands, together with the distance between Y7.43 and the three ligands were monitored to disclose the molecular mechanism of biased agonism and elucidate the role of these two residues played in the biased activation. The time evolved distances as well as the distance distributions were shown in **Figure 4A-F** . Furthermore, the conformational states of the side chains in W6.48 and Y7.43 were monitored to see how these two residues adjust the biased function of MOR (**Figure 6**).

In terms of morphine-bound MOR systems, morphine is far away from Y7.43 and does not interact with it in both wild type and mutant MORs (**Figure 1A**). All of the distances were kept stable during the MD simulations except the distance between W6.48 and Y7.43 in wild-type morphine-MOR complex, which changes from 0.6 nm to 1.0 nm after the simulation of 40 ns, and the distance was stable at ca. 0.9 nm upon the mutation W6.48L. Combining the functional assays, the W6.48L mutation reduced the degree of G-protein-bias for morphine, W6.48 is the key to adjust the G-protein bias.

In terms of fentanyl-bound MOR complex, the phenyl group in fentanyl was inserted into a small pocket between W6.48 and Y7.43, its phenyl group forms strong π-π interaction and this kind of interaction was kept during the whole simulations in both the wild-type and mutant MORs (**Figure 1B**). The distance between W6.48 and Y7.43 is stable at ca. 1.2 nm after the simulation of 40 ns in wild type MOR system, while it became stable (ca. 0.8 nm) after the simulation of 40 ns in the mutant MOR system. Upon the mutation W6.48L MOR system, Y7.43 approached to L6.48 and formed the stable hydrophobic network with the phenyl group of fentanyl. Such stable hydrophobic network is conducive to the biased β-arrestin signal, as demonstrated by the functional assays, which showed that the biased signal was strengthened (**Figure 4 H and C**).

In terms of sufentanil-bound MORs system, the phenyl group stretches into the right part of the active site in MOR since the introduction of methoxymethyl group in sufentanil results in the reorientation of phenyl group (**Figure 1C**). In addition, the phenyl is far away from Y7.43 in both the wild type and mutant systems. It is quite different from that of the fentanyl bound MOR system (**Figure 4B, C**). In contrast to the wild type MOR system, W6.48 approached to Y7.43 due to the formation of hydrophobic network in the W6.48L mutant system (**Figure 4I, L**). The functional assays showed that the signal in β-arrestin became stronger upon the W6.48L mutation within fentanyl-bound system and the signal in G-protein pathway is much stronger than that of in β-arrestin pathway in sufentanil bound W6.48L MOR system.

All evidences indicated that the stabilization of Y7.43 by ligand and the stable interactions of ligand with W6.48 and Y7.43 are propitious to the β-arrestin signal, while the stabilization of W6.48 is propitious to biased G-protein signal. Correspondingly, both the Y7.43 and W6.48 existed in the *gauch-* conformational state upon fentanyl modulated β-arrestin biased signal and existed in the *gauch+*conformational state upon the sulfentanil modulated G-protein signal (**Figure 6**).

W6.48L-induced conformational change adjusts MOR signaling bias

Through further analyzing the states of transmembrane helix in ligand-MOR systems, we found that morphine, fentanyl, sufentanil induced the different movement of helices due to the effect of 3-7 lock and the interactions with D3.32, H6.52, W6.48 and Y7.43. In morphine bound wild system, Helix 6 (H6) moved toward outside significantly (9.5 Å) and was far away from Helix 6 (H6). In fentanyl bound W6.48L mutant MOR system, H6 moved toward H5 and it moved 2.9 Å, while in sufentanil bound W6.48L mutant MOR, H6 was far away from H5 and it moved outside for 5.9 Å (**Figure 5**). Collectively, the fentanyl induced the closure of H6 towards H5 in W6.48L mutant MOR system, correspondingly, it thus transduced the β-arrestin-bias signal. In contrast to fentanyl, sufentanil made H6 away from H5, correspondingly, it transduced the G-protein-bias signal. MD simulation showed that sufentanil induced larger conformational change on MOR than that of fentanyl. It indicated that the G-protein biased agonist can induce the larger helix movement in MOR.

Discussion

In this study, we intended to find out the critical residues of μ-opioid receptor governing ligand bias by integrating computational simulations and cell assay based bias analysis. We first tried to predict the key residues influencing ligand bias at MOR by computer modeling. Then the site-directed mutation on MOR was conducted and CHO cell lines stably expressing wild-type and mutant MORs were established in order to characterize the binding affinities and functional activities of morphine and fentanyl derivatives with wild-type and mutant MORs. Based on results from functional assays, the bias profiles of morphine and fentanyl derivatives were obtained by operational model analysis. We found that D3.32 and H6.52 were critical residues in driving morphine and fentanyl derivatives to bind with μ-opioid receptor. W6.48 was a pivotal residue in governing the bias signaling of MOR. The interactions among ligand and W6.48, Y7.43 were responsible for the signaling bias. The stabilization of Y7.43 by ligand and the stable interactions of ligand with W6.48 and Y7.43 were propitious to the β-arrestin signal, while the stabilization of W6.48 is propitious to biased G-protein signal.

Recent years, unremitting efforts continually put into the research about structures of GPCR. People were trying to illustrate the mechanism underlying the activation of receptor through analysis of the structural characteristics of active receptors. It is indicated that the ligand-induced comformation of receptor is conducive to the bias signaling(*24* ,*25*). In this work, we found that the residue W6.48 and Y7.43 were paired activation switches of ligand bias at MOR, which is consistent with the computational result of Chen's work(*26*). And we proposed that the interaction between W6.48 and Y7.43 with fentanyl derivatives lead to two contrary states of transmembrane helix. When H6 moved towards H5, the "close" state impeded the activation of G-protein; When H6 moved far away from H5, the "open" state is in favour of the G-protein-dependent signaling. This is in agreement with the previous structural researches of MOR and other GPCRs. It is reported that, compared with the structure of MOR-Nb39(*15*), the TM6 of MOR-Gi is outward from TM5(*14*). The structures of other active GPCRs, such as β_2 adrenergic receptor and glucagon like peptide-1 receptor, revealed that activation always involves the relative outward movements of TM5 and TM6, which allows cavity structure for accommodating the α subunit of G-protein(*27-29*).

Opioids were used to alleviate or cure pain for centuries, but the opioid side-effects still limited their use in clinic. A great number of efforts were put in to solve the fatal hypoventilation and other adverse effects, but no completely ideal ligand was found. People have ever tried to design μ or κ subtype-selective ligands(*30* ,*31*), as well as allosteric modulators(*32*), to obtain a pain-killer without those unwanted effects, but the result is not satisfactory. Recently, the bias agonism stands a chance of separating analgesia and adverse effects for opioid ligands, the discovery of potential drugs TRV130 and PZM21 was a good signal. However, there is still a long way to go. On one hand, the mechanism of biased signaling was not clear enough. We are not sure which structural features contribute to the specific conformation of the receptor that facilitate G-protein-biased signaling. On the other hand, there is controversy in the quantification and assessment of ligand bias, the method of bias analysis was not compeletely developed. In addition, TRV130 was not approved to use clinically for its little difference of hypoventilation versus morphine in phase III study(*33*). In this study, we found the critical sites affecting ligand bias and tried to explain the mechanim of ligand bias at MOR, which contributed to better design and discovery of opioid ligands with reduced adverse effects.

Table

Table 1 pharmacological properties of test agonists for wild-type and W6.48L mutant MOR

Agonist	Wild-type					W6.48L				
	K_i(nM)	cAMP assay		βarr2 recruitment		K_i(nM)	cAMP assay		βarr2 recruitment	
		EC_{50}(nM)	Emax(%)	EC_{50}(nM)	Emax(%)		EC_{50}(nM)	Emax(%)	EC_{50}(nM)	Emax(%)
DAMGO	407.70 ± 92.07	0.81 ± 0.10	100 ± 17	8.93 ± 2.30	100 ± 12	141.5 ± 53.58	45.57 ± 11.23[d]	100 ± 7	2.86 ± 1.16	100 ± 38
Morphine	1029.00 ± 268.46	14.77 ± 1.95	104 ± 11	35.23 ± 12.75	48 ± 4	351.10 ± 40.68	333.90 ± 61.96[d]	86 ± 10	1.46 ± 0.95	81 ± 12
Fentanyl	178.10 ± 79.04	0.72 ± 0.36	111 ± 12	3.27 ± 1.43	98 ± 13	15.11 ± 18.54[a]	7.33 ± 1.87[a]	52 ± 10[d]	0.43 ± 0.15	108 ± 49
Sulfentanil	54.21 ± 13.07	0.92 ± 0.21	107 ± 6	1.01 ± 0.15	79 ± 8	0.93 ± 0.16[d]	1.02 ± 0.11	70 ± 2[d]	6.12 ± 2.27[a]	126 ± 8[d]
Remifentanil	442.10 ± 57.12	7.13 ± 1.66	127 ± 20	4.08 ± 1.38	74 ± 8	15.43 ± 3.94[d]	3.84 ± 1.32	63 ± 19[d]	0.61 ± 0.11[a]	120 ± 12[d]
3-Methyfentanyl	14.75 ± 2.80	0.15 ± 0.03	83 ± 12	0.85 ± 0.04	83 ± 12	0.41 ± 0.12[d]	0.36 ± 0.13	96 ± 9	0.01 ± 0.03[b]	138 ± 20[d]

Competition binding constant values (K_i) were determined by HTRF binding assay. The values of potency (EC_{50}) and efficacy (E_{max}, normalized to DAMGO) come from cAMP assays performed on CHO-MOR (WT & W6.48L) cells and β-arrestin2 recruitment performed on CHO-MOR (WT & W6.48L)-β-arrestin2 cells. Data were presented as mean ± SEM of three or more assays run in duplicate or triplicate. The difference between K_i, EC_{50}, and E_{max} values of wild-type versus W6.48L mutant MOR was acquired via unpaired, two-tailed t-test. The corresponding binding curves were shown in **Figure 2** , and corresponding dose-response curves were shown in **Figure 3** .

Table 2 Bias analysis of test agonists for wild-type and W6.48L mutant MOR

Agonist	Wild-type			W6.48L		
	ΔLog(τ/K_A)		ΔΔLog(τ/K_A)	ΔLog(τ/K_A)		ΔΔLog(τ/K_A)
	cAMP assay	βarr2 recruitment	cAMP/βarr2	cAMP assay	βarr2 recruitment	cAMP/βarr2
Morphine	-0.79±0.36	-2.70±0.45	1.91±0.58	-1.04±0.17	-1.38±3.02	0.34±3.02
Fentanyl	0.55±0.44	0.27±0.35	0.27±0.57	-0.75±0.46	2.15±2.83	-2.90±2.87
Sufentanil	0.46±0.36	0.14±0.56	0.32±0.67	1.25±0.22	-0.13±2.26	1.38±2.27
Remifentanil	-0.12±0.40	0.14±0.36	-0.26±0.54	-0.07±0.89	1.21±2.37	-1.28±2.53
3-Methyfentanyl	1.47±0.40	0.88±0.34	0.59±0.52	2.12±0.24	3.04±2.28	-0.92±2.30

The bias parameter ΔΔlog(τ/KA) were quantified through operational model analysis as described in the method. All data were shown as mean ± SEM of three or more assays run in triplicate. The intuitive bias comparison of wild-type versus W6.48L mutant MOR was shown in **Figure 4** .

Figure

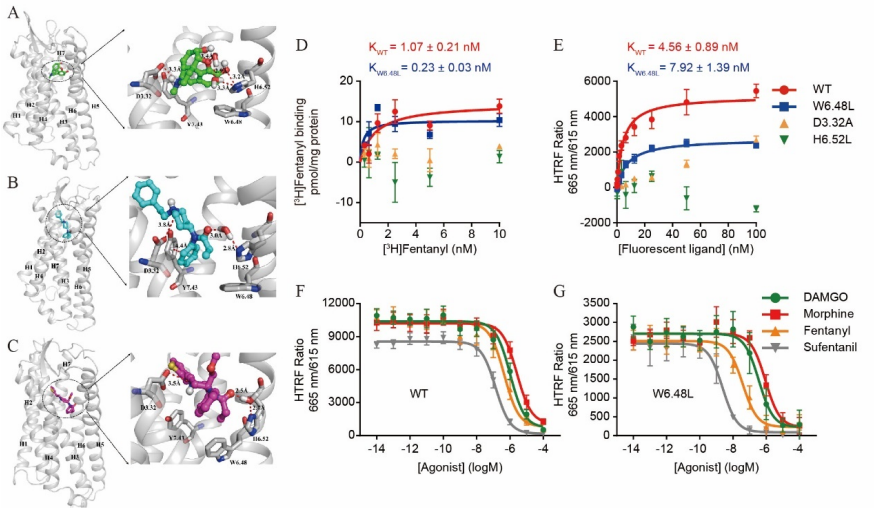

Figure 1 Site-mutations influenced binding properties of the ligand with MOR

A˜C. Details of the binding modes of (A) Morphine (67.1 ns), (B) Fentanyl (46.2 ns), (C) Sufentanil (66.4 ns)

D. Radioligand [^{3}H]Fentanyl saturation binding of wild-type and mutant MOR

E. Fluorescent ligand naltrindole saturation binding of wild-type and mutant MOR

F,G. HTRF competition binding of (F) Wild-type and (G) W6.48L mutant MOR

All data in the curves are shown as mean ± SEM of three or more assays run in duplicate, the K_i values were listed in**Table 1** .

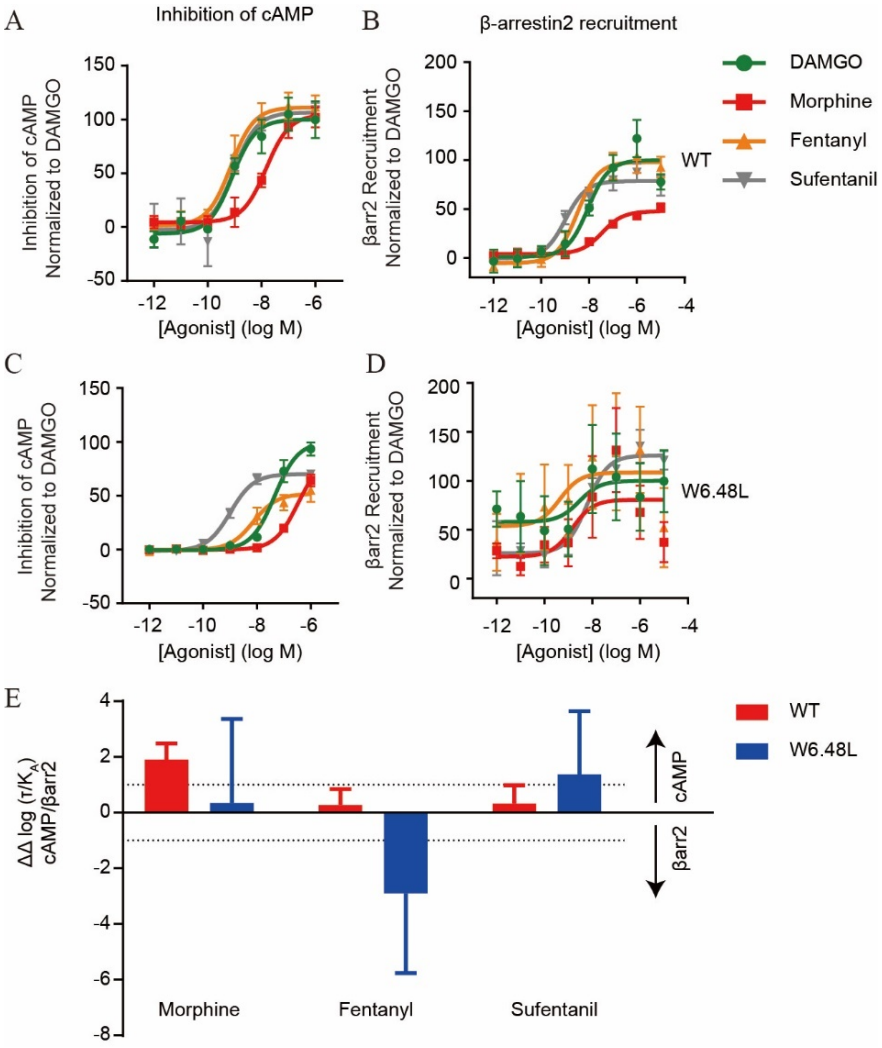

Figure 2. W6.48L mutation influenced ligand bias to stimulate MOR-mediated signaling

A, B. Inhibition of forskolin-stimulated cAMP accumulation in (A) wild-type and (B) W6.48L mutant MOR.

C, D. β-arrestin 2 translocations in (C) wild-type and (D) W6.48L mutant MOR.

E. The bias parameter ΔΔ log (τ/K_A) quantified through operational model analysis.

All data in the curves are shown as mean ± SEM of three or more assays run in triplicate, the efficacy and

potency parameters were listed in**Table 1.** The Δ log (τ/KA) and ΔΔ log (τ/KA) values were listed in **Table 2.**

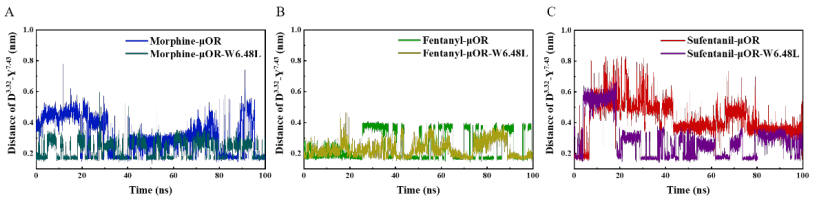

Figure 3 The distance for 3-7 lock in ligand-receptor complex systems

A. Morphine; B. Fentanyl; C. Sufentanil.

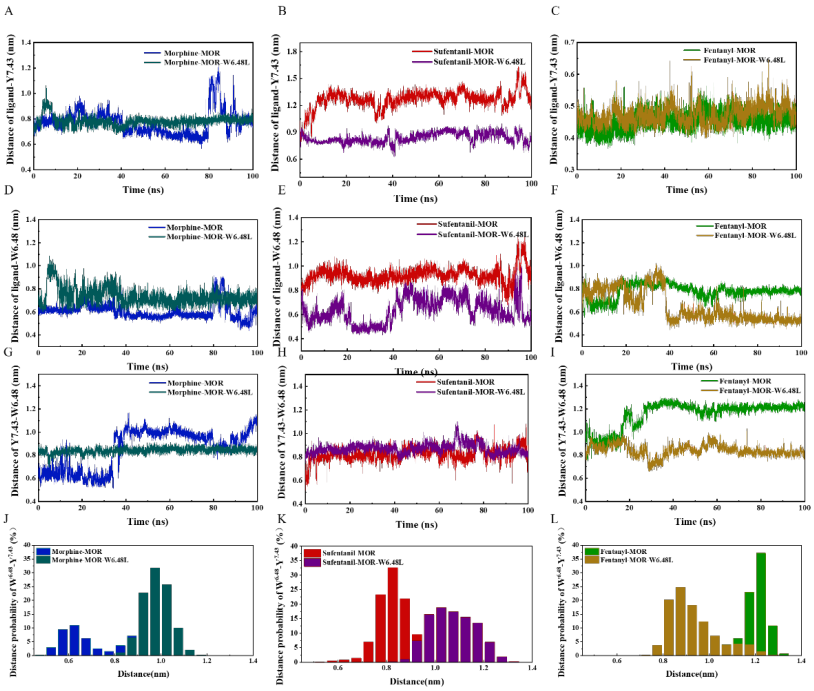

Figure 4 The distances of the ligand with residues of wild-type and W6.48L mutant receptor

The distances of ligand with A. Y7.43 in wild type and W6.48L mutant MOR bound with morphine; B. Y7.43 in wild type and W6.48L mutant MOR bound with sufentanil; C. Y7.43 in wild type and W6.48L mutant MOR bound with fentanyl; D. W6.48 in wild type and W6.48L mutant MOR bound with morphine; E. W6.48 in wild type and mutant (W6.48L) MOR bound with sufentanil; F W6.48L in wild type and W6.48L mutant MOR bound with fentanyl; The distances between Y7.43 and W6.48 in G. wild type and mutant (W6.48L) MOR bound with morphine; H. wild type and mutant (W6.48L) MOR bound with sufentanil; I. wild type and mutant (W6.48L) MOR bound with fentanyl; The Y7.43 and W6.48 distances distribution of distances in J. wild type and mutant (W6.48L) MOR bound with morphine; K. wild type and mutant (W6.48L) MOR bound with sufentanil; L. wild type and mutant (W6.48L) MOR bound with fentanyl.

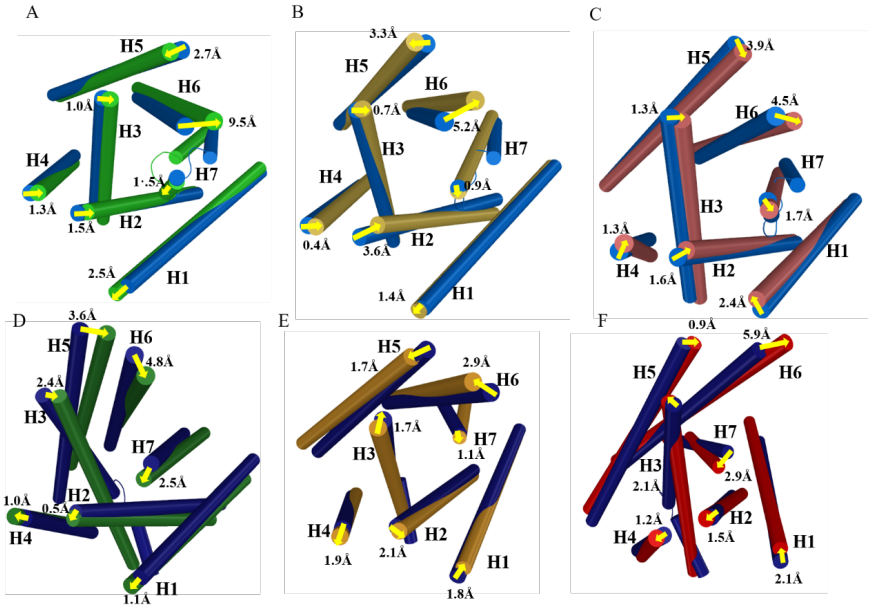

Figure 5 The transmembrane helix movements in 8 systems of ligand-bound MORs.

A. Morphine in wild type MOR B. Fentanyl in wild type MOR C. Sufentanil in wild type MOR D. Morphine in W6.48L mutant MOR E. Fentanyl in W6.48L mutant MOR F. Sufentanil in W6.48L mutant MOR.

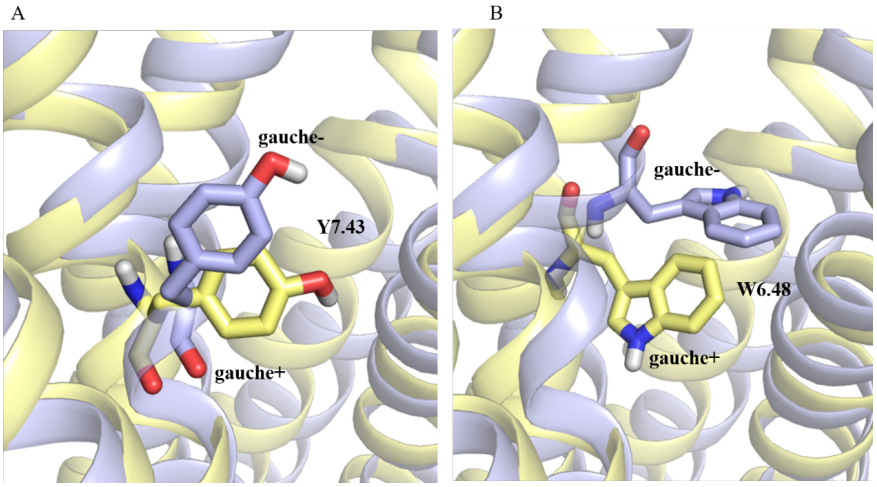

Figure 6 The conformational states of A. Y7.43 and B. W6.48 in fentanyl (blue) and sufentanil (yellow) bound MOR systems

Reference

1. Stein C (2016) Opioid Receptors.*Annual review of medicine* 67:433-451.

2. Imam MZ, Kuo A, Ghassabian S, & Smith MT (2018) Progress in understanding mechanisms of opioid-induced gastrointestinal adverse effects and respiratory depression.*Neuropharmacology* 131:238-255.

3. Zhu W, Chernew ME, Sherry TB, & Maestas N (2019) Initial Opioid Prescriptions among U.S. Commercially Insured Patients, 2012-2017. *The New England journal of medicine*380(11):1043-1052.

4. Neuman MD, Bateman BT, & Wunsch H (2019) Inappropriate opioid prescription after surgery. *Lancet (London, England)* 393(10180):1547-1557.

5. Matthes HW*, et al.* (1996) Loss of morphine-induced analgesia, reward effect and withdrawal symptoms in mice lacking the mu-opioid-receptor gene. *Nature*383(6603):819-823.

6. Bohn LM*, et al.* (1999) Enhanced morphine analgesia in mice lacking beta-arrestin 2.*Science (New York, N.Y.)* 286(5449):2495-2498.

7. Bohn LM, Gainetdinov RR, Lin FT, Lefkowitz RJ, & Caron MG (2000) Mu-opioid receptor desensitization by beta-arrestin-2 determines morphine tolerance but not dependence.*Nature* 408(6813):720-723.

8. Bohn LM, Lefkowitz RJ, & Caron MG (2002) Differential mechanisms of morphine antinociceptive tolerance revealed in (beta)arrestin-2 knock-out mice. *The Journal of neuroscience : the official journal of the Society for Neuroscience*22(23):10494-10500.

9. Raehal KM & Bohn LM (2011) The role of beta-arrestin2 in the severity of antinociceptive tolerance and physical dependence induced by different opioid pain therapeutics.*Neuropharmacology* 60(1):58-65.

10. Przewlocka B*, et al.*(2002) Knockdown of spinal opioid receptors by antisense targeting beta-arrestin reduces morphine tolerance and allodynia in rat.*Neuroscience letters* 325(2):107-110.

11. Menchine M*, et al.* (2017) Bias Factor and Therapeutic Window Correlate to Predict Safer Opioid Analgesics. *Science (New York, N.Y.)* 171(5):1165-1175.e1113.

12. Manglik A*, et al.* (2016) Structure-based discovery of opioid analgesics with reduced side effects. *Nature* 537(7619):185-190.

13. Chen XT*, et al.* (2013) Structure-activity relationships and discovery of a G protein biased mu opioid receptor ligand, [(3-methoxythiophen-2-yl)methyl]({2-[(9R)-9-(pyridin-2-yl)-6-oxaspiro-[4.5]decan- 9-yl]ethyl})amine (TRV130), for the treatment of acute severe pain.*Journal of medicinal chemistry* 56(20):8019-8031.

14. Koehl A*, et al.* (2018) Structure of the micro-opioid receptor-Gi protein complex. *Nature*558(7711):547-552.

15. Huang W*, et al.* (2015) Structural insights into micro-opioid receptor activation. *Nature*524(7565):315-321.

16. Smith JS, Lefkowitz RJ, & Rajagopal S (2018) Biased signalling: from simple switches to allosteric microprocessors. *Nature reviews. Drug discovery* 17(4):243-260.

17. Wanka L*, et al.* (2017) C-terminal motif of human neuropeptide Y4 receptor determines internalization and arrestin recruitment. *Cellular signalling*29:233-239.

18. Kenakin T & Christopoulos A (2013) Signalling bias in new drug discovery: detection, quantification and therapeutic impact. *Nature reviews. Drug discovery*12(3):205-216.

19. Weinstein JABH (1995) Integrated methods for the construction of three-dimensional models and computational probing of structure-function relations in G protein-coupled receptors. *Methods in Neurosciences* 25:366-428.

20. Black JW & Leff P (1983) Operational models of pharmacological agonism. *Proceedings of the Royal Society of London. Series B, Biological sciences*220(1219):141-162.

21. van der Westhuizen ET, Breton B, Christopoulos A, & Bouvier M (2014) Quantification of ligand bias for clinically relevant beta2-adrenergic receptor ligands: implications for drug taxonomy. *Molecular*

pharmacology 85(3):492-509.

22. Bohn LM & Aube J (2017) Seeking (and Finding) Biased Ligands of the Kappa Opioid Receptor. *ACS medicinal chemistry letters* 8(7):694-700.

23. Stott LA, Hall DA, & Holliday ND (2016) Unravelling intrinsic efficacy and ligand bias at G protein coupled receptors: A practical guide to assessing functional data.*Biochemical pharmacology* 101:1-12.

24. Staus DP*, et al.* (2016) Allosteric nanobodies reveal the dynamic range and diverse mechanisms of G-protein-coupled receptor activation. *Nature* 535(7612):448-452.

25. Manglik A & Kruse AC (2017) Structural Basis for G Protein-Coupled Receptor Activation. 56(42):5628-5634.

26. Cheng JX*, et al.* (2018) Computational insights into the G-protein-biased activation and inactivation mechanisms of the mu opioid receptor. *Acta pharmacologica Sinica* 39(1):154-164.

27. Rasmussen SG*, et al.*(2011) Crystal structure of the beta2 adrenergic receptor-Gs protein complex. *Nature* 477(7366):549-555.

28. Zhang Y*, et al.* (2017) Cryo-EM structure of the activated GLP-1 receptor in complex with a G protein. *Nature* 546(7657):248-253.

29. Liang YL*, et al.* (2017) Phase-plate cryo-EM structure of a class B GPCR-G-protein complex.*Nature* 546(7656):118-123.

30. Hughes J*, et al.* (1975) Identification of two related pentapeptides from the brain with potent opiate agonist activity. *Nature* 258(5536):577-580.

31. Gilbert PE & Martin WR (1976) The effects of morphine and nalorphine-like drugs in the nondependent, morphine-dependent and cyclazocine-dependent chronic spinal dog. *The Journal of pharmacology and experimental therapeutics*198(1):66-82.

32. Burford NT, Traynor JR, & Alt A (2015) Positive allosteric modulators of the mu-opioid receptor: a novel approach for future pain medications. *British journal of pharmacology* 172(2):277-286.

33. Anonymous (Final Summary Minutes of the Anesthetic and Analgesic Drug Products Advisory Committee Meeting October 11, 2018.

Supplementary

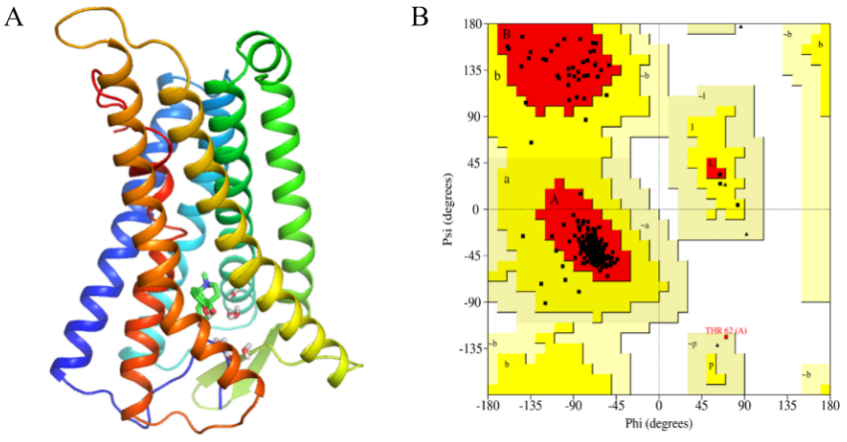

Φιγυρε Σ1 Ηομολογψ μοδελινγ οφ μ-οπιοιδ ρεχεπτορ

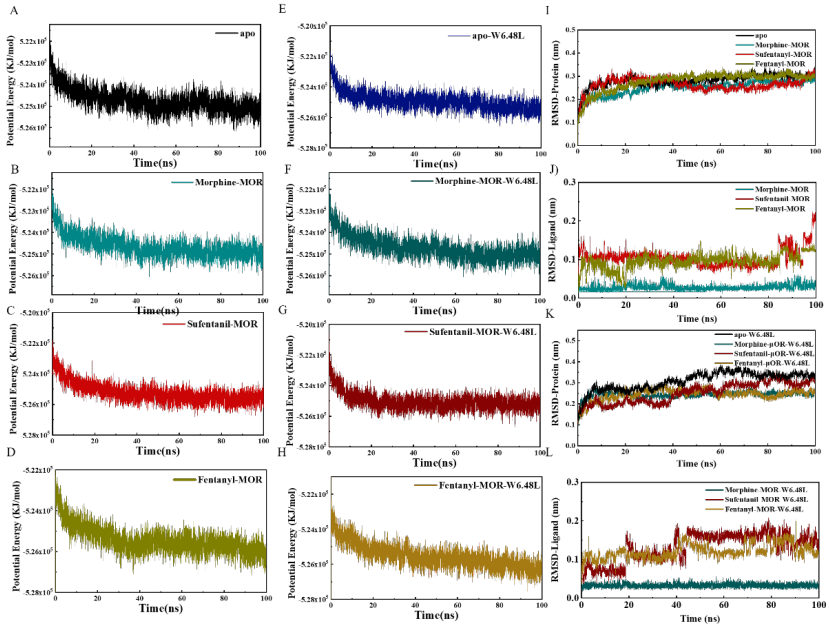

1. Structure of μ-opioid receptor
2. Ramachandran plo

Figure S2 The time evolved potential energy and RMSD

The potential energy of eight systems: A. wild type apo system, B. morphine and active MOR system, C. sulfentanil and active MOR system, D. fentanyl and active MOR system, E. MOR-W6.48L system, F. morphine and active MOR-W6.48L system, G. sulfentanil and active MOR-W6.48L system, H. fentanyl and active MOR-W6.48L system; The RMSD of wild type systems: I. protein, J. ligand; The RMSD of mutational systems: K. protein, L. ligand.

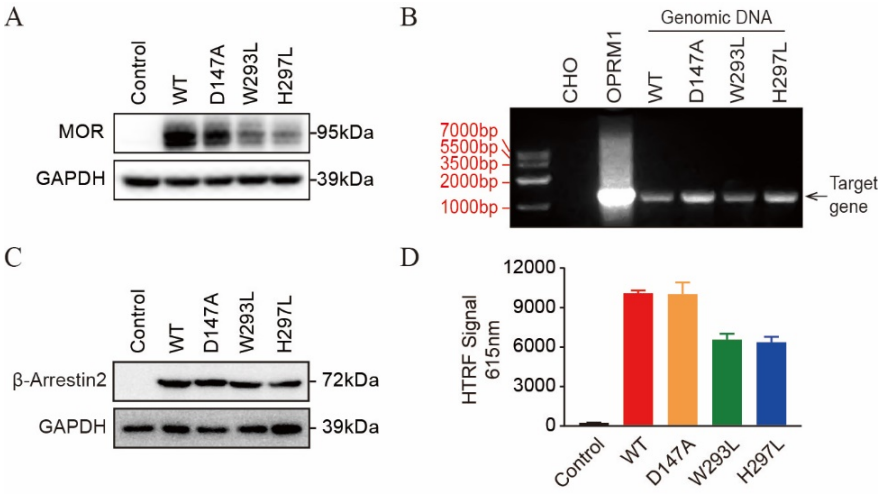

Φιγυρε Σ3 Ιδεντιφιςατιον οφ ᵀᴴᴼ σταβλψ εξπρεσσινγ MOP ςελλ λινες ανδ ᵀᴴᴼ σταβλψ εξπρεσσινγ MOP ανδ β-αρρεστιν2 ςελλ λινες.

1. Identification of MOR expression of CHO-MOR(WT & mutant) cell lines by western-blot analysis. Cells were lysed and immunoblotted with the anti-MOR antibody. To ensure equal loading into each lane, blots were also incubated with GAPDH antibody.
2. Identification of MOR mutation of CHO-MOR (WT & mutant) cell lines by PCR analysis. Genomic DNA was extracted from each CHO-MOR (WT & mutant) cell line, MOR DNA fragments were amplified from genomic DNA by PCR, then the mutant sites of MOR were confirmed by DNA sequencing.
3. Identification of β-arrestin2 expression of CHO-MOR (WT & mutant)-β-arresin2 cell lines by western-blot analysis. Cells were lysed and immunoblotted with the anti-β-arrestin2 antibody. To ensure equal loading into each lane, blots were also incubated with GAPDH antibody.
4. Identification of MOR expression on the membrane of CHO-MOR (WT & mutant) cell lines by immunofluorescence analysis. MOR on the cell membrane can be labeled with SNAP-Lumi4-Tb through incubation, then the expression level of MOR-Tb was read on Envision Multilabel Reader at 615 nm. The data are presented as mean ± SEM of three assays run in duplicate.

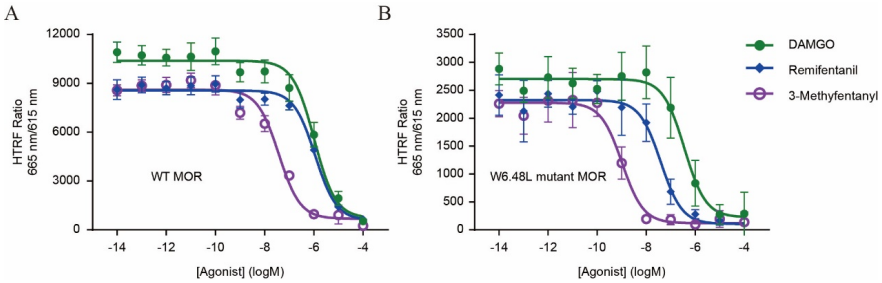

Figure S4 Competitive binding of remifentanil and 3-Methyfentanyl with wild-type and W6.48L mutant MOR.

Wild-type MOR B. W6.48L mutant MOR

All data in the curves are shown as mean ± SEM of three or more assays run in duplicate. The K_i values were listed in

Table 1.

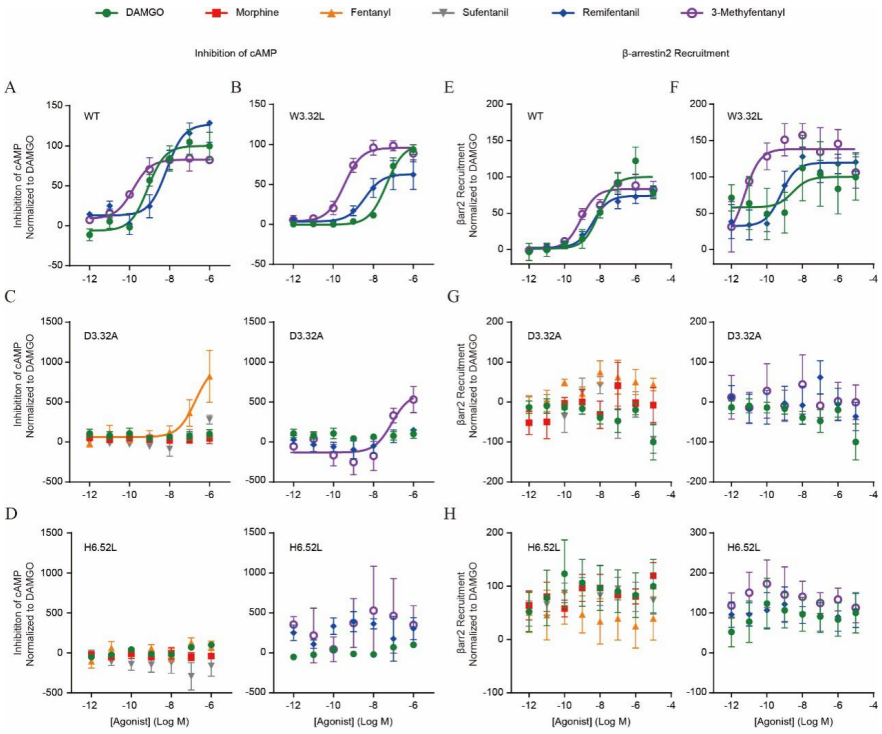

Φιγυρε Σ5 Φυνςτιοναλ αςτιιτψ οφ τεστ αγονιστς το στιμυλατε MOP-μεδιατεδ Γ-προτειν-δεπενδεντ σιγναλινγ ανδ β-αρρεστιν-δεπενδεντ σιγναλινγ

A.B. Remifentanil and 3-methyfentanyl inhibited forskolin-stimulated cAMP accumulation in (A) wild-type and (B) W6.48L mutant MOR.

C.D. Inhibition of forskolin-stimulated cAMP accumulation in (C) D3.32A and (D) H6.52L mutant MOR.

E.F. Remifentanil and 3-methyfentanyl induced β-arrestin 2 translocations in (E) wild-type and (F) W6.48L mutant MOR.

G.H. β-arrestin 2 translocations in (G) wild-type and (H) W6.48L mutant MOR.

All data in the curves are shown as mean ± SEM of three or more assays run in triplicate. The efficacy and potency parameters were listed in

Table 1.

Agonist	Wild-type					W6.48L				
	K_i(nM)	cAMP assay		βarr2 recruitment		K_i(nM)	cAMP assay		βarr2 recruitment	
		EC_{50}(nM)	Emax(%)	EC_{50}(nM)	Emax(%)		EC_{50}(nM)	Emax(%)	EC_{50}(nM)	Emax(%)
DAMGO	407.70 ± 92.07	0.81 ± 0.10	100 ± 17	8.93 ± 2.30	100 ± 12	141.5 ± 53.58	45.57 ± 11.23[d]	100 ± 7	2.86 ± 1.16	100 ± 38
Morphine	1029.00 ± 268.46	14.77 ± 1.95	104 ± 11	35.23 ± 12.75	48 ± 4	351.10 ± 40.68	333.90 ± 61.96[d]	86 ± 10	1.46 ± 0.95	81 ± 12
Fentanyl	178.10 ± 79.04	0.72 ± 0.36	111 ± 12	3.27 ± 1.43	98 ± 13	15.11 ± 18.54[a]	7.33 ± 1.87[a]	52 ± 10[d]	0.43 ± 0.15	108 ± 49
Sulfentanil	54.21 ± 13.07	0.92 ± 0.21	107 ± 6	1.01 ± 0.15	79 ± 8	0.93 ± 0.16[d]	1.02 ± 0.11	70 ± 2[d]	6.12 ± 2.27[a]	126 ± 8[d]
Remifentanil	442.10 ± 57.12	7.13 ± 1.66	127 ± 20	4.08 ± 1.38	74 ± 8	15.43 ± 3.94[d]	3.84 ± 1.32	63 ± 19[d]	0.61 ± 0.11[a]	120 ± 12[d]
3-Methyfentanyl	14.75 ± 2.80	0.15 ± 0.03	83 ± 12	0.85 ± 0.04	83 ± 12	0.41 ± 0.12[d]	0.36 ± 0.13	96 ± 9	0.01 ± 0.03[b]	138 ± 20[d]

Agonist	Wild-type			W6.48L		
	ΔLog(τ/K_A)		ΔΔLog(τ/K_A)	ΔLog(τ/K_A)		ΔΔLog(τ/K_A)
	cAMP assay	βarr2 recruitment	cAMP/βarr2	cAMP assay	βarr2 recruitment	cAMP/βarr2
Morphine	-0.79±0.36	-2.70±0.45	1.91±0.58	-1.04±0.17	-1.38±3.02	0.34±3.02
Fentanyl	0.55±0.44	0.27±0.35	0.27±0.57	-0.75±0.46	2.15±2.83	-2.90±2.87
Sufentanil	0.46±0.36	0.14±0.56	0.32±0.67	1.25±0.22	-0.13±2.26	1.38±2.27
Remifentanil	-0.12±0.40	0.14±0.36	-0.26±0.54	-0.07±0.89	1.21±2.37	-1.28±2.53
3-Methyfentanyl	1.47±0.40	0.88±0.34	0.59±0.52	2.12±0.24	3.04±2.28	-0.92±2.30